Hydrol. Earth Syst. Sci. Discuss., https://doi.org/10.5194/hess-2018-482
Manuscript under review for journal Hydrol. Earth Syst. Sci.
Discussion started: 1 November 2018

Hydrology and Earth System Sciences
Open Access
Discussions

A General Analytical Model for Head Response to Oscillatory Pumping in Unconfined Aquifers: Consider the Effects of Delayed Gravity Drainage and Initial Condition

Ching-Sheng Huang[a], Ya-Hsin Tsai[b], Hund-Der Yeh[b*] and Tao Yang[a*]

[a] State Key Laboratory of Hydrology-Water Resources and Hydraulic Engineering, Center for Global Change and Water Cycle, Hohai University, Nanjing 210098, China

[b] Institute of Environmental Engineering, National Chiao Tung University, Hsinchu 300, Taiwan

[*] Corresponding authors:

Hund-Der Yeh; E-mail: hdyeh@mail.nctu.edu.tw; Tel.: +886-3-5731910; fax: +886-3-5725958

Tao Yang; E-mail: tao.yang@hhu.edu.cn; Tel.: +86-13770918075

Key points

1. An analytical model of the hydraulic head due to oscillatory pumping in unconfined aquifers is presented.
2. Head fluctuations affected by instantaneous and delayed gravity drainages are discussed.
3. The effect of initial condition on the phase of head fluctuation is analyzed.
4. The present solution agrees well to head fluctuation data taken from a field oscillatory pumping.

Abstract

Oscillatory pumping test (OPT) is an alternative to constant-head and constant-rate pumping tests for determining aquifer hydraulic parameters without net water extraction. There is a large number of analytical models presented for the analysis of OPT. The combined effects of delayed gravity drainage (DGD) and initial condition regarding the hydraulic head are commonly neglected in the existing models. This study aims to develop a new model for describing the hydraulic head fluctuation induced by OPT in an unconfined aquifer. The model contains a groundwater flow equation with the initial condition of static water table, Neumann boundary condition specified at the rim of a finite-radius well, and a free surface equation describing water table motion with the DGD effect. The solution of the model is derived by the Laplace transform, finite integral transform, and Weber transform. Sensitivity analysis is carried out for exploring head response to the change in each of hydraulic parameters. Results suggest the DGD reduces to instantaneous gravity drainage in predicting transient head fluctuation when dimensionless parameter $a_1 = \varepsilon S_y b/\mathrm{K}_z$ exceeds 500 with empirical constant ε, specific yield S_y, aquifer thickness b, and vertical hydraulic conductivity K_z. The water table can be regarded as a no-flow boundary when $a_1 < 10^{-2}$. A pseudo-steady state model without initial condition causes a certain time shift from the actual transient model in predicting simple harmonic motion of head fluctuation during a late pumping period. In addition, the present solution agrees well to head fluctuation data observed at the Savannah River site.

KEYWORDS: oscillatory pumping test, analytical solution, free surface equation, delayed gravity drainage, initial condition

Hydrol. Earth Syst. Sci. Discuss., https://doi.org/10.5194/hess-2018-482
Manuscript under review for journal Hydrol. Earth Syst. Sci.
Discussion started: 1 November 2018

Hydrology and Earth System Sciences
Open Access
Discussions

Notation and Abbreviation

a	σ/μ
a_1, a_2	$\varepsilon S_y b/K_z$, $a_1\mu/\sigma$
b	Aquifer thickness
DGD	Delayed gravity drainage
h	Hydraulic head
$\bar{h}$	Dimensionless Hydraulic head, i.e., $\bar{h} = (2\pi l K_r h)/\lvert Q\rvert$
IGD	Instantaneous gravity drainage
K_r, K_z	Aquifer horizontal and vertical hydraulic conductivities, respectively
LHS	Left-hand side
l	Screen length, i.e., $z_u - z_l$
OPT	oscillatory pumping test
P	Period of oscillatory pumping rate
PSS	Pseudo-steady state
$\bar{P}$	Dimensionless period, i.e., $\bar{P} = (K_r P)/(S_s r_w^2)$
p	Laplace parameter
Q	Amplitude of oscillatory pumping rate
RHS	Right-hand side
r	Radial distance from the center of pumping well
$\bar{r}$	Dimensionless radial distance, i.e., $\bar{r} = r/r_w$
r_w	Radius of pumping well
SHM	Simple harmonic motion
S_s, S_y	Specific storage and specific yield, respectively
t	Time since pumping
$\bar{t}$	Dimensionless pumping time, i.e., $\bar{t} = (K_r t)/(S_s r_w^2)$
z	Elevation from aquifer bottom
z_l, z_u	Lower and upper elevations of partial well screen, respectively
$\bar{z}$	Dimensionless elevation, i.e., $\bar{z} = z/b$
$\bar{z}_l$, $\bar{z}_u$	z_l/b, z_u/b
β_n	Roots of Eqs. (19)
γ	Dimensionless frequency of oscillatory pumping rate, i.e., $S_s r_w^2\ \omega/K_r$
ε	Empirical constant associated with delayed gravity drainage
μ	$K_z r_w^2/K_r b^2$
σ	$S_y/(S_s b)$
ω	Frequency of oscillatory pumping rate, i.e., $\omega = 2\pi/P$

1. Introduction

Numerous attempts have been made by researchers to the study of oscillatory pumping test (OPT) that is an alternative to constant-rate and constant-head pumping tests for determining aquifer hydraulic parameters (e.g., Vine et al., 2016; Christensen et al., 2017; Watlet et al., 2018). The concept of OPT was first proposed by Kuo (1972) in the petroleum literature. The process of OPT contains extraction stages and injection stages. The pumping rate, in other words, varies periodically as a sinusoidal function of time. Compared with traditional constant-rate pumping, OPT in contaminated aquifers has the following advantages: (1) low cost because of no disposing contaminated water from the well, (2) reduced risk of treating contaminated fluid, (3) smaller contaminant movement, and (4) stable signal easily distinguished from background disturbance such as tide effect and varying river stage (e.g., Spane and Mackley, 2011). However, the disadvantages of OPT includes the need of an advanced apparatus producing periodic rate and the problem of signal attenuation in remote distance from the pumping well. Oscillatory hydraulic tomography adopts several oscillatory pumping wells with different frequencies (e.g., Yeh and Liu, 2000; Cardiff et al., 2013; Zhou et al., 2016; Muthuwatta, et al., 2017). Aquifer heterogeneity can be mapped by analyzing multiple data collected from observation wells. Cardiff and Barrash (2011) reviewed articles associated with hydraulic tomography and classified them according to nine categories in a table.

Various groups of researchers have worked with analytical and numerical models for OPT; each group has its own model and investigation. For example, Black and Kipp (1981) assumed the response of confined flow to OPT as simple harmonic motion (SHM) in the absence of initial condition. Cardiff and Barrash (2014) built an optimization formulation strategy using the Black and Kipp analytical solution. Dagan and Rabinovich (2014) also assumed hydraulic head fluctuation as SHM for OPT at a partially penetrating well in unconfined aquifers. Cardiff et al. (2013) characterized aquifer heterogeneity using the finite element-based COMSOL software that adopts SHM hydraulic head variation for OPT. On the other hand, Rasmussen et al. (2003) found hydraulic head response tends to SHM after a certain period of pumping time when considering initial condition prior to OPT. Bakhos et al. (2014) used the Rasmussen et al. (2003) analytical solution to quantify the time after which hydraulic head fluctuation can be regarded as SHM since OPT began. As mentioned above, most of the models for OPT assume hydraulic head fluctuation as SHM without initial condition, and all of them treat the pumping well as a line source with infinitesimal radius.

Field applications of OPT for determining aquifer parameters have been conducted in recent years. Rasmussen et al. (2003) estimated aquifer hydraulic parameters based on 1- or 2-hour period of OPT at the Savannah River site. Maineult et al. (2008) observed spontaneous potential temporal variation in aquifer diffusivity at a study site in Bochum, Germany. Fokker et al. (2012; 2013) presented spatial distributions of aquifer transmission and storage coefficient derived from curve fitting based on a numerical model and field data from experiments at the southern city-limits of Bochum, Germany. Rabinovich et al. (2015) estimated aquifer parameters of equivalent hydraulic conductivity, specific storage and specific yield at the Boise Hydrogeophysical Research Site by curve fitting based on observation data and the Dagan and Rabinovich (2014) analytical solution. They conclude the equivalent hydraulic parameters can represent the actual aquifer heterogeneity of the study site.

Although a large number of studies have been made in developing analytical models for OPT, little is known about the combined effects of delayed gravity drainage (DGD), finite-radius pumping well, and initial condition prior to OPT. Analytical solution to such a question will not only have important physical implications but also shed light on OPT model development. This study builds an improved model describing hydraulic head fluctuation induced by OPT in an unconfined aquifer. The model is composed of a typical flow equation with the initial condition of static water table, an inner boundary condition specified at the rim of the pumping well for incorporating finite-radius effect, and a free surface equation describing the motion of water table with the DGD effect. The analytical solution of the model

Hydrol. Earth Syst. Sci. Discuss., https://doi.org/10.5194/hess-2018-482
Manuscript under review for journal Hydrol. Earth Syst. Sci.
Discussion started: 1 November 2018

Hydrology and Earth System Sciences
Open Access
Discussions

is derived by the methods of Laplace transform, finite integral transform, and Weber transform. Based on the present solution, sensitivity analysis is performed to explore the hydraulic head in response to the change in each of hydraulic parameters. The effects of DGD and instantaneous gravity drainage (IGD) on the head fluctuations are compared. The quantitative criterion for treating the well radius as infinitesimal is discussed. The effect of the initial condition on the phase of head fluctuation is investigated. In addition, curve fitting of the present solution to head fluctuation data recorded at the Savannah River site is presented.

2. Methodology

2.1. Mathematical model

Consider an OPT in an unconfined aquifer illustrated in Fig. 1. The aquifer is of unbound lateral extent with a finite thickness b. The radial distance from the centerline of the well is r; an elevation from the impermeable bottom of the aquifer is z. The well with outer radius r_w is screened from z_u to z_l.

The flow equation describing spatiotemporal head distribution in aquifers can be written as:

$$K_r\left(\frac{\partial^2 h}{\partial r^2}+\frac{1}{r}\frac{\partial h}{\partial r}\right)+K_z\frac{\partial^2 h}{\partial z^2}=S_s\frac{\partial h}{\partial t} \quad \text{for} \quad r_w \le r < \infty,\ 0 \le z \le b \quad \text{and} \quad t \ge 0 \qquad (1)$$

where $h(r,z,t)$ is hydraulic head at location (r, z) and time t; K_r and K_z are respectively the radial and vertical hydraulic conductivities; S_s is the specific storage. Consider water table as a reference datum where the elevation head is set to zero; the initial condition is expressed as:

$$h = 0 \text{ at } t = 0 \qquad (2)$$

The rim of the wellbore is regarded as an inner boundary under the Neumann condition expressed as:

$$2\pi r_w K_r l\frac{\partial h}{\partial r}=\begin{cases} Q\sin(\omega t) & \text{for} \quad z_l \le z \le z_u \\ 0 & \text{outside screen interval} \end{cases} \quad \text{at} \quad r{=}r_w \qquad (3)$$

where $l = z_u - z_l$ is screen length; Q and $\omega = 2\pi/P$ are respectively the amplitude and

Hydrol. Earth Syst. Sci. Discuss., https://doi.org/10.5194/hess-2018-482
Manuscript under review for journal Hydrol. Earth Syst. Sci.
Discussion started: 1 November 2018

frequency of oscillatory pumping rate (i.e., $Q\sin(\omega t)$) with a period P. Water table motion can be defined by Eq. (4a) for IGD (Neuman, 1972) and Eq. (4b) for DGD (Moench, 1995).

$$K_z \frac{\partial h}{\partial z} = -S_y \frac{\partial h}{\partial t} \quad \text{at} \quad z = b \ \text{ for IGD} \tag{4a}$$

$$K_z \frac{\partial h}{\partial z} = -\varepsilon \ S_y \int_0^t \frac{\partial h}{\partial t'} \exp(-\varepsilon(t - t'))\, \mathrm{d}t' \quad \text{at} \quad z = b \ \text{ for DGD}$$

(4b)

where S_y is the specific yield; ε is an empirical constant. The impervious aquifer bottom is under the no-flow condition:

$$\frac{\partial h}{\partial z} = 0 \quad \text{at} \quad z = 0 \tag{5}$$

The hydraulic head far away from the pumping well remains constant, written as

$$\lim_{r \to \infty} h(r, z, t) = 0 \tag{6}$$

Define dimensionless variables and parameters as follows:

$$\bar{h} = \frac{2\pi l K_r}{Q} h,\ \bar{r} = \frac{r}{r_w},\ \bar{z} = \frac{z}{b},\ \bar{z}_l = \frac{z_l}{b},\ \bar{z}_u = \frac{z_u}{b},\ \bar{t} = \frac{K_r}{S_s r_w^2} t,\ \bar{P} = \frac{K_r}{S_s r_w^2} P$$

$$\gamma = \frac{S_s r_w^2}{K_r} \omega,\ \mu = \frac{K_z r_w^2}{K_r b^2},\ \sigma = \frac{S_y}{S_s b}\ , a = \frac{\sigma}{\mu},\ a_1 = \frac{\varepsilon S_y b}{K_z},\ a_2 = \frac{a_1 \mu}{\sigma} \tag{7}$$

where the overbar stands for a dimensionless symbol. Note that the magnitude of a_1 is related to the DGD effect (Moench, 1995) and γ is a dimensionless frequency parameter. With Eq. (7), the dimensionless forms of Eqs. (1) - (6) become, respectively,

$$\frac{\partial^2 \bar{h}}{\partial \bar{r}^2} + \frac{1}{\bar{r}} \frac{\partial \bar{h}}{\partial \bar{r}} + \mu \frac{\partial^2 \bar{h}}{\partial \bar{z}^2} = \frac{\partial \bar{h}}{\partial \bar{t}} \quad \text{for} \quad 1 \le \bar{r} < \infty,\ 0 \le \bar{z} < 1 \quad \text{and} \quad \bar{t} \ge 0 \tag{8}$$

$$\bar{h} = 0 \quad \text{at} \quad \bar{t} = 0 \tag{9}$$

$$\frac{\partial \bar{h}}{\partial \bar{r}} = \begin{cases} \sin(\gamma \bar{t}) & \text{for} \quad \bar{z}_l \le \bar{z} \le \bar{z}_u \\ 0 & \text{outside screen interval} \end{cases} \quad \text{at} \quad \bar{r} = 1 \tag{10}$$

$$\frac{\partial \bar{h}}{\partial \bar{z}} = -a \frac{\partial \bar{h}}{\partial \bar{t}} \quad \text{at} \quad \bar{z} = 1 \ \text{ for IGD} \tag{11a}$$

$$\frac{\partial \bar{h}}{\partial \bar{z}} = -a_1 \int_0^{\bar{t}} \frac{\partial \bar{h}}{\partial \bar{t}'} \exp(-a_2(\bar{t} - \bar{t}'))\, d\bar{t}' \quad \text{at} \quad \bar{z} = 1 \ \text{ for DGD} \tag{12b}$$

$$\frac{\partial \bar{h}}{\partial \bar{z}} = 0 \quad \text{at} \quad \bar{z} = 0 \tag{13}$$

$$\lim_{\bar{r} \to \infty} \bar{h}(\bar{r}, \bar{z}, \bar{t}) = 0 \tag{14}$$

Eqs. (8) – (13) represent the transient DGD model when excluding (11a) and transient IGD model when excluding (11b).

2.2. Transient solution for unconfined aquifer

The Laplace transform and finite integral transform are applied to solve Eqs. (8) - (13) (Liang et al., 2017). The former converts $\bar{h}(\bar{r},\bar{z},\bar{t})$ into $\hat{h}(\bar{r},\bar{z},p)$, $\partial\bar{h}/\partial\bar{t}$ in Eq. (8), (11) into $p\hat{h}$, and $\sin(\gamma\bar{t})$ in Eq. (10) into $\gamma/(p^2+\gamma^2)$ with the Laplace parameter *p*. The result of Eq. (8) in the Laplace domain can be written as

$$\frac{\partial^2\hat{h}}{\partial\bar{r}^2}+\frac{1}{\bar{r}}\frac{\partial\hat{h}}{\partial\bar{r}}+\mu\frac{\partial^2\hat{h}}{\partial\bar{z}^2}=p\hat{h} \tag{14}$$

The transformed boundary conditions in *r* and *z* directions are expressed as

$$\frac{\partial\hat{h}}{\partial\bar{r}}=\begin{cases}\frac{\gamma}{p^2+\gamma^2} & \text{for} \quad \bar{z}_l\le\bar{z}\le\bar{z}_u \\ 0 & \text{outside screen interval}\end{cases} \quad \text{at} \quad \bar{r}=1 \tag{15}$$

$$\frac{\partial\hat{h}}{\partial\bar{z}}=-ap\hat{h} \quad \text{at} \quad \bar{z}=1 \ \text{ for IGD} \tag{16a}$$

$$\frac{\partial\hat{h}}{\partial\bar{z}}=-\frac{a_1p\hat{h}}{p+a_2} \quad \text{at} \quad \bar{z}=1 \ \text{ for DGD} \tag{16b}$$

$$\frac{\partial\hat{h}}{\partial\bar{z}}=0 \quad \text{at} \quad \bar{z}=0 \tag{17}$$

$$\lim_{\bar{r}\to\infty}\hat{h}(\bar{r},\bar{z},p)=0 \tag{18}$$

The finite integral transform proposed by Latinopoulos (1985) is applied to Eqs. (14) - (17). The definition of the transform is given in Appendix A. Using the property of the transform converts $\hat{h}(\bar{r},\bar{z},p)$ into $\tilde{h}(\bar{r},\beta_n,p)$ and $\partial^2\hat{h}/\partial\bar{z}^2$ in Eq. (14) into $-\beta_n^2\tilde{h}$ with $n\in(1,2,3,\ldots\infty)$ and β_n being the positive roots of the equation:

$$\tan\beta_n=c/\beta_n \tag{19}$$

where $c=ap$ for IGD and $a_1p/(p+a_2)$ for DGD. The method to find the roots of β_n is discussed in section 2.3. Eq. (14) then becomes an ordinary differential equation (ODE) denoted as

$$\frac{\partial^2\tilde{h}}{\partial\bar{r}^2}+\frac{1}{\bar{r}}\frac{\partial\tilde{h}}{\partial\bar{r}}-\mu\beta_n^2\tilde{h}=p\tilde{h} \tag{20}$$

with the transformed Eqs. (18) and (15) written, respectively, as

Hydrol. Earth Syst. Sci. Discuss., https://doi.org/10.5194/hess-2018-482
Manuscript under review for journal Hydrol. Earth Syst. Sci.
Discussion started: 1 November 2018

Hydrology and Earth System Sciences
Open Access
Discussions

$$\lim_{\bar{r}\to\infty} \tilde{h}(\bar{r},\beta_n,p) = 0 \tag{21a}$$

$$\frac{\partial \tilde{h}}{\partial \bar{r}} - \alpha p \tilde{h} = \frac{\gamma\ F_t}{\beta_n(p^2+\gamma^2)}\left(\sin(\bar{z}_u\beta_n) - \sin(\bar{z}_l\beta_n)\right) \quad \text{at} \quad \bar{r} = 1 \tag{21b}$$

where $F = \sqrt{2(\beta_n^2 + c^2)/(\beta_n^2 + c^2 + c)}$. Note that the transformation from Eq. (14) to (20) is applicable only for the no-flow condition specified at $\bar{z} = 0$ (i.e., Eq. (17)) and third-type condition specified at $\bar{z} = 1$ (i.e., Eq. (16a) or (16b)). Solve Eq. (20) with (21a) and (21b), and we can obtain:

$$\tilde{h}(\bar{r},\beta_n,p) = -\frac{\gamma\ FK_0(r\lambda)(\sin(\bar{z}_u\beta_n)-\sin(\bar{z}_l\beta_n))}{\beta_n\lambda K_1(\lambda)(p^2+\gamma^2)} \tag{22}$$

with

$$\lambda = \sqrt{p + \mu\ \ \beta_n^2} \tag{23}$$

where $K_0(-)$ and $K_1(-)$ is the modified Bessel function of the second kind of order zero and one, respectively. Applying the inverse Laplace transform and inverse finite integral transform to Eq. (22) results in the transient solution expressed as

$$\bar{h}(\bar{r},\bar{z},\bar{t}) = \bar{h}_{\mathrm{exp}}(\bar{r},\bar{z},\bar{t}) + \bar{h}_{\mathrm{SHM}}(\bar{r},\bar{z},\bar{t}) \tag{24a}$$

with

$$\bar{h}_{\mathrm{exp}}(\bar{r},\bar{z},\bar{t}) = \frac{-2\gamma}{\pi}\sum_{n=1}^{\infty}\int_0^{\infty} \cos(\beta_n\bar{z})\exp(p_0\bar{t})\,\mathrm{Im}(\varepsilon_1\varepsilon_2)\ \ d\zeta \tag{24b}$$

$$\bar{h}_{\mathrm{SHM}}(\bar{r},\bar{z},\bar{t}) = \bar{A}_t(\bar{r},\bar{z})\cos\left(\gamma\bar{t} - \phi_t(\bar{r},\bar{z})\right) \tag{24c}$$

$$\bar{A}_t(\bar{r},\bar{z}) = \sqrt{a_t(\bar{r},\bar{z})^2 + b_t(\bar{r},\bar{z})^2} \tag{24d}$$

$$a_t(\bar{r},\bar{z}) = \frac{2}{\pi}\sum_{n=1}^{\infty}\int_0^{\infty} p_0\cos(\beta_n\bar{z})\,\mathrm{Im}(\varepsilon_1\varepsilon_2)\,d\zeta \tag{24e}$$

$$b_t(\bar{r},\bar{z}) = \frac{2\gamma}{\pi}\sum_{n=1}^{\infty}\int_0^{\infty} \cos(\beta_n\bar{z})\,\mathrm{Im}(\varepsilon_1\varepsilon_2)\,d\zeta \tag{24f}$$

$$\phi_t(\bar{r},\bar{z}) = \cos^{-1}\left(b_t(\bar{r},\bar{z})/\bar{A}_t(r,\bar{z})\right) \tag{24g}$$

$$\varepsilon_1 = K_0(\lambda_0\bar{r})(\sin(\bar{z}_u\beta_n) - \sin(\bar{z}_l\beta_n))/(\beta_n\lambda_0K_1(\lambda_0)(p_0^2 + \gamma^2)) \tag{24h}$$

$$\varepsilon_2 = (\beta_n^2 + c_0^2)/(\beta_n^2 + c_0^2 + c_0) \tag{24i}$$

$$p_0 = -\zeta - \mu\beta_n^2 \tag{24j}$$

$$\lambda_0 = \sqrt{\zeta}i \tag{24k}$$

Hydrol. Earth Syst. Sci. Discuss., https://doi.org/10.5194/hess-2018-482
Manuscript under review for journal Hydrol. Earth Syst. Sci.
Discussion started: 1 November 2018

where $c_0 = ap_0$ for IGD and $a_1 p_0/(p_0 + a_2)$ for DGD, i is the imaginary unit, and Im(-) is the imaginary part of a complex number. The detailed derivation of Eqs. (24a) – (24k) is presented in Appendix B. The first term on the right-hand side (RHS) of Eq. (24a) exhibits exponential decay due to the initial condition since pumping began; the second term defines SHM with amplitude $\bar{A}_t(\bar{r}, \bar{z})$ and phase shift $\phi_t(\bar{r}, \bar{z})$ at a given point $(\bar{r}, \bar{z})$. The numerical results of the integrals in Eqs. (24b), (24e) and (24f) are obtained by the Mathematica NIntegrate function.

2.3. Calculation of β_n

The eigenvalues $\beta_1, \ldots, \beta_n$, the roots of Eq. (19) with $c = c_0$ can be determined by applying the Mathematica function FindRoot based on Newton's method with reasonable initial guesses. The roots are located at the intersection of the curves plotted by the RHS and left-hand side (LHS) functions of β_n in Eq. (19). The roots are very close to the vertical asymptotes of the periodical tangent function $\tan \beta_n$. When $c_0 = ap_0$, the initial guess for each β_n can be considered as $\beta_{0,n} + \delta$ where $\beta_{0,n} = (2n-1)\pi/2$, $n \in (1,2,\ldots\infty)$ and δ is a small positive value set to 10^{-10} to prevent the denominator in Eq. (19) from zero. When $c_0 = a_1 p_0/(p_0 + a_2)$, the initial guess is set to $\beta_{0,n} - \delta$ for $a_2 - \zeta \leq 0$. There is an additional vertical asymptote at $\beta_n = \sqrt{(a_2 - \zeta)/\mu}$ derived from the RHS function of Eq. (19) if $a_2 - \zeta > 0$. The initial guess is therefore set to $\beta_{0,n} + \delta$ for $\beta_{0,n}$ on the LHS of the asymptote and $\beta_{0,n} - \delta$ for $\beta_{0,n}$ on the RHS.

2.4. Transient solution for confined aquifer

When $S_y = 0$ (i.e., $a = 0$ or $a_1 = 0$), Eq. (11a) or (11b) reduces to $\partial\bar{h}/\partial\bar{z} = 0$ for no-flow condition at the top of the aquifer, indicating the unconfined aquifer becomes a confined one. Under this condition, Eq. (19) becomes $\tan \beta_n = 0$ with roots $\beta_n = 0, \pi, 2\pi, \ldots, n\pi, \ldots, \infty$; Eq. (24i) reduces to $\varepsilon_2 = 1$; factor 2 in Eqs. (24b), (24e) and (24f) is replaced by unity for $\beta_n = 0$ and remains for the others. The analytical solution of the transient head for the confined aquifer can be expressed as Eqs. (24a) - (24k) with

$$\bar{h}_{\exp}(\bar{r},\bar{z},\bar{t}) = \frac{-\gamma}{\pi}\int_0^\infty \mathrm{Im}(\varepsilon_0)\ \exp(-\zeta\bar{t})\,d\zeta - \frac{2\gamma}{\pi}\sum_{n=1}^{\infty}\int_0^\infty \cos(n\pi\bar{z})\,\mathrm{Im}(\varepsilon_1)\exp(p_0\bar{t})\ d\zeta \tag{25a}$$

$$a_t(\bar{r},\bar{z}) = -\frac{1}{\pi}\int_0^\infty \zeta\mathrm{Im}(\varepsilon_0)\,d\zeta + \frac{2}{\pi}\sum_{n=1}^{\infty}\int_0^\infty p_0\cos(n\pi\bar{z})\,\mathrm{Im}(\varepsilon_1)\,d\zeta \tag{25b}$$

$$b_t(\bar{r},\bar{z}) = \frac{\gamma}{\pi}\int_0^\infty \mathrm{Im}(\varepsilon_0)\,d\zeta + \frac{2\gamma}{\pi}\sum_{n=1}^{\infty}\int_0^\infty \cos(n\pi\bar{z})\,\mathrm{Im}(\varepsilon_1)\,d\zeta \tag{25c}$$

$$\varepsilon_0 = (\bar{z}_u - \bar{z}_l)K_0(\lambda_0\bar{r})/(\lambda_0 K_1(\lambda_0)(\zeta^2+\gamma^2)) \tag{25d}$$

Note that Eq. (24h) reduces to Eq. (25d) based on $\beta_n = 0$ and L' Hospital's rule. When $\bar{z}_u = 1$ and $\bar{z}_l = 0$ for the case of full screen, Eq. (24) gives $\varepsilon_1 = 0$ for $\beta_n > 0$ and the second RHS terms of Eqs. (25a) – (25c) can therefore be eliminated. This causes the solution for confined aquifers is independent of dimensionless elevation $\bar{z}$, indicating only horizontal flow in the aquifer.

2.5. Pseudo-steady state solution for unconfined aquifer

A pseudo-steady state (PSS) solution $\bar{h}_s$ accounts for SHM of head fluctuation after a certain period of pumping time and satisfies the following form (Dagan and Rabinovich, 2014)

$$\bar{h}_s(\bar{r},\bar{z},\bar{t}) = \mathrm{Im}\left(\bar{H}(\bar{r},\bar{z})\ e^{i\gamma\bar{t}}\right) \tag{26}$$

where $\bar{H}(\bar{r},\bar{z})$ is a space function of $\bar{r}$ and $\bar{z}$. Define a PSS IGD model as Eqs. (8) - (13) excluding (9), (11b) and replacing $\sin(\gamma\bar{t})$ in (10) by $e^{i\gamma\bar{t}}$. Substituting Eq. (26) and $\partial\bar{h}_s/\partial\bar{t} = \mathrm{Im}\left(i\gamma\bar{H}(\bar{r},\bar{z})\ e^{i\gamma\bar{t}}\right)$ into the model results in

$$\frac{\partial^2\bar{H}}{\partial\bar{r}^2} + \frac{1}{\bar{r}}\frac{\partial\bar{H}}{\partial\bar{r}} + \mu\frac{\partial^2\bar{H}}{\partial\bar{z}^2} = i\gamma\bar{H} \tag{27}$$

$$\frac{\partial\bar{H}}{\partial\bar{r}} = \begin{cases} 1 & \text{for} \quad \bar{z}_l \le \bar{z} \le \bar{z}_u \\ 0 & \text{outside screen interval} \end{cases} \quad \text{at} \quad \bar{r} = 1 \tag{28}$$

$$\frac{\partial\bar{H}}{\partial\bar{z}} = -ia\gamma\bar{H} \quad \text{at} \quad \bar{z} = 1 \ \text{ for IGD} \tag{29}$$

$$\frac{\partial\bar{H}}{\partial\bar{z}} = 0 \quad \text{at} \quad \bar{z} = 0 \tag{30}$$

$$\lim_{\bar{r}\to\infty}\bar{H} = 0 \tag{31}$$

The resultant model is independent of $\bar{t}$, indicating the analytical solution of $\bar{H}(\bar{r},\bar{z})$ is

Hydrol. Earth Syst. Sci. Discuss., https://doi.org/10.5194/hess-2018-482
Manuscript under review for journal Hydrol. Earth Syst. Sci.
Discussion started: 1 November 2018

Hydrology and Earth System Sciences
Open Access
Discussions

tractable. Similarly, consider a PSS DGD model that equals the PSS IGD model but replaces (11a) by (11b). Substituting Eq. (26) into the result yields a model that depends on $\bar{t}$, indicating the solution $\bar{h}_s$ to the PSS DGD model is not tractable.

Taking the Weber transform to Eqs. (27) - (31) converts $\bar{H}$ into $\tilde{H}$ and $\partial^2\bar{H}/\partial r^2 + r^{-1}\partial\bar{H}/\partial r$ into $-\xi^2\tilde{H} - 2/(\pi\xi)\partial\bar{H}/\partial r|_{r=1}$. The result is expressed as

$$\frac{\partial^2\tilde{H}}{\partial\bar{z}^2} - \lambda_w^2\tilde{H} = \begin{cases} 0 & \text{for} \quad \bar{z}_u < \bar{z} \leq 1 \\ \frac{2}{\pi\mu\xi} & \text{for} \quad \bar{z}_l \leq \bar{z} \leq \bar{z}_u \\ 0 & \text{for} \quad 0 \leq \bar{z} < \bar{z}_l \end{cases} \tag{32}$$

$$\frac{\partial\tilde{H}}{\partial\bar{z}} = -i\alpha\gamma\tilde{H} \quad \text{at} \quad \bar{z} = 1 \tag{33}$$

$$\frac{\partial\tilde{H}}{\partial\bar{z}} = 0 \quad \text{at} \quad \bar{z} = 0 \tag{34}$$

where $\lambda_w^2 = (\xi^2 + i\gamma)/\mu$ and ξ is the Weber parameter. One can refer to Appendix C for the definition of the transform. Eq. (32) can be separated as

$$\begin{cases} \partial^2\tilde{H}_u/\partial\bar{z}^2 - \lambda_w^2\tilde{H}_u = 0 \quad \text{for} \quad \bar{z}_u < \bar{z} \leq 1 \\ \partial^2\tilde{H}_m/\partial\bar{z}^2 - \lambda_w^2\tilde{H}_m = 2/(\pi\mu\xi) \quad \text{for} \quad \bar{z}_l \leq \bar{z} \leq \bar{z}_u \\ \partial^2\tilde{H}_l/\partial\bar{z}^2 - \lambda_w^2\tilde{H}_l = 0 \quad \text{for} \quad 0 \leq \bar{z} < \bar{z}_l \end{cases} \tag{35}$$

with the continuity requirements:

$$\begin{cases} \tilde{H}_m = \tilde{H}_u \\ \partial\tilde{H}_m/\partial\bar{z} = \partial\tilde{H}_u/\partial\bar{z} \end{cases} \quad \text{at} \quad \bar{z} = \bar{z}_u \tag{36}$$

$$\begin{cases} \tilde{H}_l = \tilde{H}_m \\ \partial\tilde{H}_l/\partial\bar{z} = \partial\tilde{H}_m/\partial\bar{z} \end{cases} \quad \text{at} \quad \bar{z} = \bar{z}_l \tag{37}$$

Solving Eq. (35) with (33), (34), (36), and (37) results in

$$\begin{cases} \tilde{H}_u = \tilde{H}_p(c_1\exp(\lambda_w\bar{z}) + c_2\exp(-\lambda_w\bar{z})) \quad \text{for} \quad \bar{z}_u < \bar{z} \leq 1 \\ \tilde{H}_m = \tilde{H}_p(c_3\exp(\lambda_w\bar{z}) + c_4\exp(-\lambda_w\bar{z}) - 1) \quad \text{for} \quad \bar{z}_l \leq \bar{z} \leq \bar{z}_u \\ \tilde{H}_l = \tilde{H}_p c_5(\exp(\lambda_w\bar{z}) + \exp(-\lambda_w\bar{z})) \quad \text{for} \quad 0 \leq \bar{z} < \bar{z}_l \end{cases} \tag{38a}$$

with

$$c_1 = -e^{-\lambda_w}(\lambda_w - \alpha)(\sinh(\bar{z}_l\lambda_w) - \sinh(\bar{z}_u\lambda_w))/D \tag{38b}$$

$$c_2 = -e^{\lambda_w}(\lambda_w + \alpha)(\sinh(\bar{z}_l\lambda_w) - \sinh(\bar{z}_u\lambda_w))/D \tag{38c}$$

$$c_3 = \frac{e^{-(1+\bar{z}_l+\bar{z}_u)\lambda_w}}{2D}\Big(\alpha\big(e^{(2+\bar{z}_l)\lambda_w} + e^{\bar{z}_u\lambda_w} - e^{(2\bar{z}_l+\bar{z}_u)\lambda_w}\big) + (\alpha - \lambda_w)e^{(\bar{z}_l+2\bar{z}_u)\lambda_w} +$$

Hydrol. Earth Syst. Sci. Discuss., https://doi.org/10.5194/hess-2018-482
Manuscript under review for journal Hydrol. Earth Syst. Sci.
Discussion started: 1 November 2018

$$\lambda_w(e^{(2+\bar{z}_l)\lambda_w} - e^{\bar{z}_u\lambda_w} + e^{(2\bar{z}_l+\bar{z}_u)\lambda_w})) \tag{38d}$$

$$c_4 = \frac{e^{-(1+\bar{z}_l+\bar{z}_u)\lambda_w}}{2D}\Big((\alpha - \lambda_w)e^{(\bar{z}_l+2\bar{z}_u)\lambda_w} + (\alpha + \lambda_w)(e^{(2+\bar{z}_l)\lambda_w} - e^{(2+\bar{z}_u)\lambda_w} + e^{(2+2\bar{z}_l+\bar{z}_u)\lambda_w})\Big) \tag{38e}$$

$$c_5 = \frac{1}{2}e^{-(1+\bar{z}_l+\bar{z}_u)\lambda_w}(e^{\bar{z}_l\lambda_w} - e^{\bar{z}_u\lambda_w})((\lambda_w - \alpha)e^{(\bar{z}_l+\bar{z}_u)\lambda_w} + (\lambda_w + \alpha)e^{2\lambda_w}) \tag{38f}$$

where $\alpha = i\gamma a$, $\widetilde{H}_p = 2/(\pi\mu\xi\lambda_w^2)$ and $D = 2(\alpha\cosh\lambda_w + \lambda_w\sinh\lambda_w)$. The solution of $\overline{H}$ given below can be obtained by the formula for the inverse Weber transform shown in Appendix C.

$$\overline{H}(\bar{r},\bar{z}) = \begin{cases} \int_0^\infty \widetilde{H}_u\ \xi\ \Omega\ d\xi & \text{for}\quad \bar{z}_u < \bar{z} \le 1 \\ \int_0^\infty \widetilde{H}_m\ \xi\ \Omega\ d\xi & \text{for}\quad \bar{z}_l \le \bar{z} \le \bar{z}_u \\ \int_0^\infty \widetilde{H}_l\ \xi\ \Omega\ d\xi & \text{for}\quad 0 \le \bar{z} < \bar{z}_l \end{cases} \tag{39a}$$

$$\Omega = \big(J_0(\xi\bar{r})Y_1(\xi) - Y_0(\xi\bar{r})J_1(\xi)\big)/\big(J_1^2(\xi) + Y_1^2(\xi)\big) \tag{39b}$$

with the Bessel functions of the first kind of order zero $J_0(-)$ and one $J_1(-)$ as well as the second kind of order zero $Y_0(-)$ and $Y_1(-)$. Note that the solution reduces to $\overline{H}(\bar{r},\bar{z}) = \int_0^\infty \widetilde{H}_m\ \xi\ \Omega\ d\xi$ for a fully screened well when $\bar{z}_l = 0$ and $\bar{z}_u = 1$. With Eq. (26) and the formula of $e^{i\gamma\bar{t}} = \cos(\gamma\bar{t}) + i\sin(\gamma\bar{t})$, the solution of $\bar{h}_s$ is expressed as

$$\bar{h}_s(\bar{r},\bar{z},\bar{t}) = \bar{A}_s(\bar{r},\bar{z})\cos\big(\gamma t - \phi_s(\bar{r},\bar{z})\big) \tag{40a}$$

$$\bar{A}_s(\bar{r},\bar{z}) = \sqrt{a_s(\bar{r},\bar{z})^2 + b_s(\bar{r},\bar{z})^2} \tag{40b}$$

$$a_s(\bar{r},\bar{z}) = \mathrm{Re}\big(\overline{H}(\bar{r},\bar{z})\big) \tag{40c}$$

$$b_s(\bar{r},\bar{z}) = \mathrm{Im}\big(\overline{H}(\bar{r},\bar{z})\big) \tag{40d}$$

$$\phi_s(\bar{r},\bar{z}) = \cos^{-1}\big(b_s(\bar{r},\bar{z})/A_s(\bar{r},\bar{z})\big) \tag{40e}$$

where Re(-) is the real part of a complex number. Eq. (40a) indicates SHM for the response of the hydraulic head at any point to oscillatory pumping.

2.6. Pseudo-steady state solution for confined aquifers

Applying the finite Fourier cosine transform to the model, Eqs. (27) – (31) with $S_y = 0$ (i.e., $a = 0$) for the confined condition converts $\overline{H}$ into $\acute{H}$ and $\partial^2\overline{H}/\partial\bar{z}^2$ into $(m\pi)^2\acute{H}$ with m

Hydrol. Earth Syst. Sci. Discuss., https://doi.org/10.5194/hess-2018-482
Manuscript under review for journal Hydrol. Earth Syst. Sci.
Discussion started: 1 November 2018

being an integer from 0, 1, 2, … ∞. The result is written as

$$\frac{\partial^2 \acute{H}}{\partial \bar{r}^2} + \frac{1}{\bar{r}}\frac{\partial \acute{H}}{\partial \bar{r}} - \lambda_m^2 \acute{H} = 0 \tag{41}$$

$$\frac{\partial \acute{H}}{\partial \bar{r}} = \begin{cases} \bar{z}_u - \bar{z}_l & \text{for} \quad m = 0 \\ \frac{1}{m\pi}(\sin(\bar{z}_u m\pi) - \sin(\bar{z}_l m\pi)) & \text{for} \quad m > 0 \end{cases} \quad \text{at} \quad \bar{r} = 1 \tag{42}$$

$$\lim_{\bar{r}\to\infty} \acute{H} = 0 \tag{43}$$

where $\lambda_m^2 = \gamma i + \mu(m\pi)^2$; the result for $m = 0$ is derived by L' Hospital's. Solve Eq. (41) with (42) and (43), and we can have

$$\acute{H}(\bar{r}) = \frac{-K_0(\bar{r}\lambda_m)}{\lambda_m K_1(\lambda_m)} \times \begin{cases} \bar{z}_u - \bar{z}_l & \text{for} \quad m = 0 \\ \frac{1}{m\pi}(\sin(\bar{z}_u m\pi) - \sin(\bar{z}_l m\pi)) & \text{for} \quad m > 0 \end{cases} \tag{44}$$

After applying the inversion to Eq. (44) and the formula of $e^{i\gamma\bar{t}} = \cos(\gamma\bar{t}) + i\sin(\gamma\bar{t})$, the solution of $\bar{h}_s$ for confined aquifers can be expressed as Eqs. (40a) - (40e) with $\bar{H}(\bar{r},\bar{z})$ replaced by

$$\bar{H}(\bar{r},\bar{z}) = -2\sum_{m=0}^{\infty} \frac{K_0(\bar{r}\lambda_m)}{\lambda_m K_1(\lambda_m)} \times \begin{cases} 0.5(\bar{z}_u - \bar{z}_l) & \text{for} \quad m = 0 \\ \frac{\cos(m\pi\bar{z})}{m\pi}(\sin(\bar{z}_u m\pi) - \sin(\bar{z}_l m\pi)) & \text{for} \quad m > 0 \end{cases} \tag{45}$$

For a fully screened well (i.e., $\bar{z}_u = 1$, $\bar{z}_l = 0$), the first term of the series (i.e., $m = 0$) remains and the others equal zero because of $\sin(\bar{z}_u m\pi) - \sin(\bar{z}_l m\pi) = 0$. The result is independent of dimensionless elevation $\bar{z}$, indicating the confined flow is only horizontal.

2.7. Special cases of the present solution

Table 1 classifies the present solution (i.e., solution 1) and its special cases (i.e., solutions 2 to 6) according to transient or PSS flow, unconfined or confined aquifer, and IGD or DGD. Each of solutions 1 to 6 reduces to a special case for fully screened well. Existing analytical solutions can be regarded as special cases of the present solution as discussed in section 3.4 (e.g., Black and Kipp, 1981; Rasmussen et al., 2003; Dagan and Rabinovich, 2014).

2.8. Sensitivity analysis

Sensitivity analysis evaluates hydraulic head variation in response to the change in each of K_r, K_z, S_s, S_y, ω, and ε. The normalized sensitivity coefficient can be defined as (Liou and Yeh, 1997)

$$S_i = P_i \frac{\partial X}{\partial P_i} \tag{46}$$

where S_i is the sensitivity coefficient of ith parameter; P_i is the magnitude of the ith input parameter; X represents the present solution in dimensional form. Eq. (46) can be approximated as

$$S_i = P_i \frac{X(P_i+\Delta P_i)-X(P_i)}{\Delta P_i} \tag{47}$$

where ΔP_i, a small increment, is chosen as $10^{-3}P_i$.

3. Results and Discussion

The following sections demonstrate the response of the hydraulic head to oscillatory pumping using the present solution. The default values in calculation are r = 0.05 m, z = 5 m, t = 0, b = 10 m, $Q = 10^{-3}$ m^3/s, r_w = 0.05 m, z_u = 5.5 m, z_l = 4.5 m, $K_r = 10^{-4}$ m/s, $K_z = 10^{-5}$ m/s, $S_s = 10^{-5}$ m^{-1}, $S_y = 10^{-4}$, $\omega = 2\pi/30$ s^{-1}, and $\varepsilon = 10^{-2}$ s^{-1}. The corresponding dimensionless parameters and variables are $\bar{r} = 1$, $\bar{z} = 0.5$, $\bar{t} = 0$, $\bar{z}_u = 0.55$, $\bar{z}_l = 0.45$, $\gamma = 5.24\times10^{-5}$, $\mu = 2.5 \times 10^{-6}$, $\alpha = 4 \times 10^5$, $a_1 = 1$ and $a_2 = 2.5 \times 10^{-6}$.

3.1. Delayed gravity drainage

Previous analytical models for OPT consider either confined flow (e.g., Rasmussen et al., 2003) or unconfined flow with IGD effect (e.g., Dagan and Rabinovich, 2014). Little attention has been given to the DGD effect. This section examines the relation between these three kinds of models. Figure 2 shows the curve of the dimensionless amplitude $\bar{A}_t$ at ($\bar{r}$, $\bar{z}$) = (1, 1) of solution 1 versus the dimensionless parameter a_1 related to the effect. The transient head fluctuations are plotted by solution 1 with $a_1 = 10^{-2}$, 1, 10, 500, solution 2 for IGD and solution 3 for confined flow. When $10^{-2} \le a_1 \le 500$, the $\bar{A}_t$ gradually decreases with a_1 to the trough and then increases to the ultimate value of $\bar{A}_t = 1.79 \times 10^{-2}$. The DGD, in other words, causes an effect. When $a_1 \le 10^{-2}$, solutions 1 and 3 agree on the predicted heads, indicating the unconfined aquifer with the DGD effect behaves like confined aquifer and the water table can be regarded as a no-flow boundary. When $a_1 \geq 500$, the head fluctuations predicted by solutions 1 and 2 are identical, indicating the DGD effect can be ignored and Eq. (4b) reduces to (4a) for the IGD condition.

3.2. Effect of finite radius of pumping well

Existing analytical models for OPT mostly treated the pumping well as a line source with infinitesimal radius (e.g., Rasmussen et al., 2003; Dagan and Rabinovich, 2014). The finite difference scheme for the model also treats the well as a nodal point by neglecting the radius. These will lead to significant error when a well has the radius ranging from 0.5 m to 2 m (Yeh and Chang, 2013). This section discusses the relative error in predicted amplitude defined as

$$RE = |\bar{A}_{D\&R} - \bar{A}_t|/\bar{A}_t \tag{48}$$

where $\bar{A}_{D\&R}$ and $\bar{A}_t$ are the dimensionless amplitudes at $\bar{r} = 1$ (i.e., $r = r_w$) predicted by the Dagan and Rabinovich (2014) solution and the IGD solution 2. Note that their solution assumes infinitesimal radius of a pumping well and has a typo that the term $e^{-D_w+1} - e^{-D_w}$ should read $e^{\beta(-D_w+1)} - e^{-\beta D_w}$ (see their Eq. (25)). Figure 3 demonstrates the RE for different values of radius r_w. The RE increases with r_w as expected. For case 1 of r_w = 0.1 m, both solutions agree well in the entire domain of $1 \leq \bar{r} \leq \infty$, indicating a pumping well with $r_w \leq$ 0.1 m can be regarded as a line source. For the extreme case 2 of r_w = 1 m or case 3 of r_w = 2 m, the Dagan and Rabinovich solution underestimates the dimensionless amplitude for $1 \leq \bar{r} \leq 6$ and agrees to the present solution for $\bar{r} > 6$. The REs for these two cases exceed 10%. The effect of finite radius should therefore be considered in OPT models especially when observed hydrulic head data are taken close to the wellbore of a large-diameter well.

3.3. Sensitivity analysis

The temporal distributions of normalized sensitivity coefficient S_i defined as Eq. (47) with $X = h_{\exp}$ of solution 1 are displayed in Fig. 4a for the response of exponential decay to the change in each of six parameters K_r, K_z, S_s, S_y, ω and ε. The exponential decay is very sensitive to variation in each of K_r, K_z, S_s and ω because of $|S_i| > 0$. Precisely, a positive perturbation

Hydrol. Earth Syst. Sci. Discuss., https://doi.org/10.5194/hess-2018-482
Manuscript under review for journal Hydrol. Earth Syst. Sci.
Discussion started: 1 November 2018

in S_s produces an increase in the magnitude of h_{exp} while that in K_r or K_z causes a decrease. In addition, a positive perturbation in ω yields an increase in h_{exp} before $t = 1$ s and a decrease after that time. It is worth noting that S_i for S_y or ε is very close to zero over the entire period of time, indicating h_{exp} is insensitive to the change in S_y or ε and the subtle change of gravity drainage has no influence on the exponential decay. On the other hand, the spatial distributions of S_i associated with the amplitude A_t are shown in Fig. 4b in response to the changes in those six parameters. The A_t is again sensitive to the change in each of K_r, K_z, S_s and ω but insensitive to the change in S_y or ε. The same result of $|S_i| \cong 0$ for S_y or ε applies to any observation point under the water table (i.e., $\bar{z} < 1$), but $|S_i| > 0$ at the water table (i.e., $\bar{z} = 1$) shown in Fig. 4c. From those discussed above, we may conclude the changes in the four key parameters K_r, K_z, S_s and ω significantly affect head prediction in the entire aquifer domain. The change in S_y or ε leads to insignificant variation in the predicted head below the water table and slight variation at the water table.

3.4. Transient head fluctuation affected by the initial condition

Figure 5 demonstrates head fluctuations predicted by DGD solution 1 and IGD solution 2 expressed as $\bar{h} = \bar{h}_{\mathrm{exp}} + \bar{h}_{\mathrm{SHM}}$ for transient flow and by IGD solution as $\bar{h}_s = \bar{A}_s \cos(\gamma t - \phi_s)$ for PSS flow. The transient head fluctuation starts from $\bar{h} = 0$ at $\bar{t} = 0$ and approaches SHM predicted by $\bar{h}_{\mathrm{SHM}}$ when $\bar{h}_{\mathrm{exp}} \cong 0$ m after $\bar{t} = 0.5\bar{P}$ (i.e., 6×10^4). Solutions 1 and 2 agree to the $\bar{h}$ predictions because the head at $\bar{z} = 0.5$ under the water table is insensitive to the change in S_y or ε as discussed in section 3.3. It is worth noting that the solution of Dagan and Rabinovich (2014) for PSS flow has a certain time shift from the $\bar{h}_{\mathrm{SHM}}$ of solution 2. This indicates the phase of their solution (i.e., 1.50 rad) should be replaced by the phase of solution 2 (i.e., $\phi_t = 1.64$ rad) so that their solution exactly fits the $\bar{h}_{\mathrm{SHM}}$ of solution 2.

Figure 6 displays head fluctuations predicted by transient solution 3 expressed as $\bar{h} = \bar{h}_{\mathrm{exp}} + \bar{h}_{\mathrm{SHM}}$ and PSS solution 6 as $\bar{h}_s = \bar{A}_s \cos(\gamma t - \phi_s)$ for partially-screened pumping well in panel (a) and full screen in panel (b). The Rasmussen et al. (2003) solution for transient flow predicts the same $\bar{h}$ as solution 3. The Black and Kipp (1981) for PPS flow also predict close $\bar{h}_{\mathrm{SHM}}$ predictions of solution 3. The phase of solution 6 (i.e., ϕ_s = 1.50 rad for panel (a) and 1.33 rad for (b)) should also be replaced by the phase of solution 3 (i.e., $\phi_t = 1.64$ rad for (a) and 1.81 rad for (b)) so that both solutions 3 and 6 agree to the SHM of head fluctuation. As concluded, excluding the initial condition with Eq. (26) for a PSS model leads to a certain time shift from the SHM of the head fluctuation predicted by the associated transient model while the transient and PSS models give the same SHM amplitude.

3.5. Application of the present solution to field experiment

Rasmussen et al. (2003) conducted field OPTs in a three-layered aquifer system containing one Surficial Aquifer, the Barnwell-McBean Aquifer in between and the deepest Gordon Aquifer at the Savannah River site. Two clay layers dividing these three aquifers may be regarded as impervious strata. For the OPT at the Surficial Aquifer, the formation has 6.25 m averaged thickness near the test site. The fully-screened pumping well has 7.6 cm outer radius. The pumping rate can be approximated as $Q\sin(\omega t)$ with $Q = 4.16\times10^{-4}$ m^3/s and $\omega = 2\pi$ h^{-1}. The distance from the pumping well is 6 m to the observation well 101D and 11.5 m to well 102D. The screen lengths are 3 m from the aquifer bottom for well 101D and from the water table for well 102D. For the OPT at the Barnwell-McBean Aquifer, the formation mainly consists of sand and fine-grained material. The pumping well has outer radius of 7.6 cm and pumping rate of $Q\sin(\omega t)$ with $Q = 1.19\times10^{-3}$ m^3/s and $\omega = \pi$ h^{-1}. The observation well 201C is at 6 m from the pumping well. The data of time-varying hydraulic heads at the observation wells (i.e., 101D, 102D, 201C) are plotted in Fig. 7. One can refer to Rasmussen et al. (2003) for detailed description of the Savannah River site.

The aquifer hydraulic parameters are determined based on solutions 3 to 6 coupled with the Levenberg–Marquardt algorithm provided in the Mathematica function FindFit (Wolfram, 1991). Solutions 4 and 5 are used to predict depth-averaged head expressed as

$(z_u' - z_l')^{-1} \int_{z_l'}^{z_u'} h_s dz$ with the upper elevation z_u' and lower one z_l' of the finite screen of the observation well 101D or 102D at the Surficial Aquifer. Note that solutions 3 and 6 are independent of elevation because of the fully-screened pumping well. Define the standard error of estimate (SEE) as $\mathrm{SEE} = \sqrt{\frac{1}{M}\sum_{j=1}^{M} e_j^2}$ and the mean error (ME) as $\mathrm{ME} = \frac{1}{M}\sum_{j=1}^{M} e_j$ where e_j is the difference between predicted and observed hydraulic heads and M is the number of observation data (Yeh, 1987). The estimated parameters and associated SEE and ME are displayed in Table 2. The result shows the estimated S_y is very small, and the estimated T and S by solution 3 or 6 for confined flow are close to those by solution 4 or 5 for unconfined flow, indicating that the unconfined flow induced by the OPT in the Surficial Aquifer is negligibly small. Little gravity drainage due to the DGD effect appears with a_1 = 20 for wells 101D and 102D as discussed in section 3.1. Rasmussen et al. (2003) also revealed the confined behaviour of the OPT-induced flow in the Surficial Aquifer. The estimated S_y is one order less than the lower limit of the typical range of 0.01 ~ 0.3 (Freeze and Cherry, 1979), which accords with the findings of Rasmussen et al. (2003) and Rabinovich et al. (2015). Such a fact might be attributed to the problem of the moisture exchange limited by capillary fringe between the zones below and upper the water table. Several laboratory researches have confirmed an estimate of S_y at short period of OPT is much smaller than that determined by constant-rate pumping test (e.g., Cartwright et al., 2003; 2005). On the other hand, transient solution 3 gives smaller SEEs than PSS solution 6 for the Barnwell-McBean Aquifer and better fits to the observed data at the early pumping periods as shown in Fig. 7. From those discussed above, we may conclude the present solution is applicable to real-world OPT.

4. Concluding remarks

A variety of analytical models for OPT have been proposed so far, but little attention is paid to the joint effects of DGD, initial condition, and finite radius of a pumping well. This study develops a new model for describing hydraulic head fluctuation due to OPT in unconfined

Hydrol. Earth Syst. Sci. Discuss., https://doi.org/10.5194/hess-2018-482
Manuscript under review for journal Hydrol. Earth Syst. Sci.
Discussion started: 1 November 2018

aquifers. Static hydraulic head prior to OPT is regarded as an initial condition. A Neumann boundary condition is specified at the rim of a finite-radius pumping well. A free surface equation accounting for the DGD effect is considered as the top boundary condition. The solution of the model is derived by the Laplace transform, finite integral transform and Weber transform. The sensitivity analysis of the head response to the change in each of hydraulic parameters is performed. The observation data obtained from the OPT at the Savannah River site are analyzed by the present solution when coupling the Levenberg–Marquardt algorithm to estimate aquifer hydraulic parameters. Our findings are summarized below:

1. When $10^{-2} \leq a_1 \leq 500$, the effect of DGD on the head fluctuation should be considered. The amplitude of head fluctuation predicted by DGD solution 1 decreases with increasing a_1 to a certain trough and then increases to the amplitude predicted by IGD solution 2. When $a_1 > 500$, the DGD becomes IGD. Both solutions 1 and 2 predict the same head fluctuation. When $a_1 < 10^{-2}$, the DGD results in the water table under no-flow condition. Solution 1 for unconfined flow gives an identical head prediction to solution 3 for confined flow.
2. Assuming a large-diameter well as a line source with infinitesimal radius underestimates the amplitude of head fluctuation in the domain of $1 \leq \bar{r} \leq 6$ when the radius exceeds 80 cm, leading to relative error RE > 10% shown in Fig. 3. In contrast, the assumption is valid in predicting the amplitude in the domain of $\bar{r} > 6$ in spite of adopting a large-diameter well. When $r_w \leq 10$ cm (i.e., RE < 0.45%), the well radius can be regarded as infinitesimal. The result is applicable to existing analytical solutions assuming infinitesimal radius and finite difference solutions treating the pumping well as a nodal point.
3. The sensitivity analysis suggests the changes in four parameters K_r, K_z, S_s and ω significantly affect head prediction in the entire aquifer domain. The change in S_y or ε causes insignificant variation in the head under water table but slight variation at the water table.

Hydrol. Earth Syst. Sci. Discuss., https://doi.org/10.5194/hess-2018-482
Manuscript under review for journal Hydrol. Earth Syst. Sci.
Discussion started: 1 November 2018

4. Analytical solutions for OPT are generally expressed as the sum of the exponential and harmonic functions of time (i.e., $\bar{h} = \bar{h}_{\mathrm{exp}} + \bar{A}_t \cos(\gamma t - \phi_t)$) for transient solutions (e.g., solution 3) and harmonic function (i.e., $\bar{h}_\mathrm{s} = \bar{A}_s \cos(\gamma t - \phi_s)$) for PSS solutions (e.g., solution 6). The latter assuming Eq. (26) without the initial condition produces a certain time shift from the SHM predicted by the $\bar{h}_{\mathrm{SHM}}$. The phase ϕ_s should be replaced by ϕ_t so that $\bar{h}_\mathrm{s}$ and $\bar{h}_{\mathrm{SHM}}$ are exactly the same.

References

Bakhos, T., Cardiff, M., Barrash, W., and Kitanidis, P. K.: Data processing for oscillatory pumping tests, J. Hydrol., 511, 310–319, 2014.

Black, J. H., and Kipp, K. L.: Determination of hydrogeological parameters using sinusoidal pressure tests - a theoretical appraisal, Water Resour. Res., 17(3), 686–692, 1981.

Cardiff, M., Bakhos, T., Kitanidis, P. K., and Barrash, W.: Aquifer heterogeneity characterization with oscillatory pumping: Sensitivity analysis and imaging potential, Water Resour. Res., 49(9), 5395–5410, 2013.

Cardiff, M. and Barrash, W.: 3-D transient hydraulic tomography in unconfined aquifers with fast drainage response, Water Resour. Res., 47: W12518, 2011.

Cardiff, M. and Barrash, W.: Analytical and semi‐analytical tools for the design of oscillatory pumping tests, Ground Water, 53(6), 896–907, 2014.

Cartwright, N., Nielsen, P., and Dunn, S.: Water table waves in an unconfined aquifer: Experiments and modeling, Water Resour. Res., 39(12), 1330, 2003.

Cartwright, N., Nielsen, P., and Perrochet, P.: Influence of capillarity on a simple harmonic oscillating water table: Sand column experiments and modeling, Water Resour. Res., 41(8), W08416, 2005.

Christensen, N. K., Ferre, T. P. A., Fiandaca, G., and Christensen, S.: Voxel inversion of airborne electromagnetic data for improved groundwater model construction and prediction

Hydrol. Earth Syst. Sci. Discuss., https://doi.org/10.5194/hess-2018-482
Manuscript under review for journal Hydrol. Earth Syst. Sci.
Discussion started: 1 November 2018

Hydrology and Earth System Sciences
Open Access
Discussions

accuracy, Hydrol. Earth Syst. Sci., 21, 1321–1337, 2017.

Dagan, G. and Rabinovich, A.: Oscillatory pumping wells in phreatic, compressible, and homogeneous aquifers, Water Resour. Res., 50(8), 7058–7066, 2014.

Fokker, P. A., Salina Borello, E., Serazio, C., and Verga, F.: Estimating reservoir heterogeneities from pulse testing, J. Petrol. Sci. Eng., 86–87, 15–26, 2012.

Fokker, P. A., Renner, J., and Verga, F.: Numerical modeling of periodic pumping tests in wells penetrating a heterogeneous aquifer, Am. J. Environ. Sci, 9(1), 1–13, 2013.

Freeze, R. A. and Cherry, J. A.: Groundwater, Prentice-Hall, New Jersey, 1979, 604 pp.

Kuo, C.: Determination of reservoir properties from sinusoidal and multirate flow tests in one or more wells, SPE J., 12(6), 499–507, 1972.

Latinopoulos, P.: Analytical solutions for periodic well recharge in rectangular aquifers with 3rd-kind boundary-conditions, J. Hydrol., 77(1–4), 293–306, 1985.

Liang, X., Zhan, H., Zhang, Y.-K., and Liu, J.: On the coupled unsaturated-saturated flow process induced by vertical, horizontal, and slant wells in unconfined aquifers, Hydrol. Earth Syst. Sci., 21, 1251–1262, 2017.

Liou, T. S., and Yeh, H. D.: Conditional expectation for evaluation of risk groundwater flow and solute transport: one-dimensional analysis, J. Hydrol., 199, 378–402, 1997.

Maineult, A., Strobach, E., and Renner, J.: Self-potential signals induced by periodic pumping tests, J. Geophys. Res: Sol. Earth, 113(B1), B01203, 2008.

Moench, A. F.: Combining the Neuman and Boulton models for flow to a well in an unconfined aquifer, Ground Water, 33(3), 378–384, 1995.

Muthuwatta, L., Amarasinghe, U. A., Sood, A., and Surinaidu, L.: Reviving the "Ganges Water Machine": where and how much?, Hydrol. Earth Syst. Sci., 21, 2545–2557, 2017.

Neuman, S.P.: Theory of flow in unconfined aquifers considering delayed response of the water table, Water Resour. Res., 8(4), 1031–1045, 1972.

Rabinovich, A., Barrash, W., Cardiff, M., Hochstetler, D., Bakhos, T., Dagan, G., and Kitanidis,

P. K.: Frequency dependent hydraulic properties estimated from oscillatory pumping tests in an unconfined aquifer, J. Hydrol., 531, 2–16, 2015.

Rasmussen, T. C., Haborak, K. G., and Young, M. H.: Estimating aquifer hydraulic properties using sinusoidal pumping at the Savannah River site, South Carolina, USA, Hydrogeol. J., 11(4), 466–482, 2003.

Spane, F. A. and Mackley, R. D.: Removal of river-stage fluctuations from well response using multiple regression, Ground Water, 49(6), 794–807, 2011.

Vine, N. L., Butler, A., McIntyre, N., and Jackson, C.: Diagnosing hydrological limitations of a land surface model: application of JULES to a deep-groundwater chalk basin, Hydrol. Earth Syst. Sci., 20, 143–159, 2016.

Watlet, A., Kaufmann, O., Triantafyllou, A., Poulain, A., Chambers, J. E., Meldrum, P. I., Wilkinson, P. B., Hallet, V., Quinif, Y., Ruymbeke, M. V., and Camp, M. V.: Imageing groundwater infiltration dynamics in the karst vadose zone with long-term ERT monitoring, Hydrol. Earth Syst. Sci., 22, 1563–1592, 2018.

Wolfram, S.: Mathematica, Version 2.0. Wolfram Research, Inc., Champaign, IL, 1991.

Yeh, H. D.: Theis' solution by nonlinear least ‐ squares and finite ‐ difference Newton's Method, Ground Water, 25(6), 710–715, 1987.

Yeh, T. C. J. and Liu, S. Y.: Hydraulic tomography: Development of a new aquifer test method, Water Resour. Res., 36(8), 2095–2105, 2000.

Zhou, Y. Q., Lim, D., Cupola, F., and Cardiff, M.: Aquifer imaging with pressure waves evaluation of low-impact characterization through sandbox experiments, Water Resour. Res., 52(3), 2141–2156, 2016.

Acknowledgments

Research leading to this paper has been partially supported by the grants from the Fundamental Research Funds for the Central Universities (2018B00114), the National Natural Science

Foundation of China (41561134016 and 51421006) and the Taiwan Ministry of Science and Technology under the contract numbers MOST 107-2221-E-009-019-MY3. The authors are grateful to Prof. T. C. Rasmussen for kindly providing the OPT data obtained from the Savannah River site.

Appendix A: Finite integral transform

Applying the finite integral transform to $\hat{h}$ of the model, Eqs. (14) – (18), results in (Latinopoulos, 1985)

$$\tilde{h}(\beta_n) = \Im\{\hat{h}(\bar{z})\} = \int_0^1 \hat{h}(\bar{z})\ F\cos(\beta_n \bar{z})\, d\bar{z} \tag{A.1}$$

$$F = \sqrt{\frac{2(\beta_n^2 + c^2)}{\beta_n^2 + c^2 + c}} \tag{A.2}$$

where β_n is the root of Eq. (19). On the basis of integration by parts, one can write

$$\Im\left\{\frac{\partial^2 \hat{h}}{\partial \bar{z}^2}\right\} = \int_0^1 \left(\frac{\partial^2 \hat{h}}{\partial \bar{z}^2}\right) F\cos(\beta_n z)\, d\bar{z} = -\beta_n^2 \tilde{h} \tag{A.3}$$

Note that Eq. (A.3) is applicable only for the no-flow condition specified at $\bar{z} = 0$ (i.e., Eq. (17)) and third-type condition specified at $\bar{z} = 1$ (i.e., Eq. 16a or 16b). The formula for the inverse finite integral transform is defined as

$$\hat{h}(\bar{z}) = \Im^{-1}\{\tilde{h}(\beta_n)\} = \sum_{n=1}^{\infty} \tilde{h}(\beta_n) F\cos(\beta_n \bar{z}) \tag{A.4}$$

Appendix B: Derivation of Eqs. (24a) – (24k)

On the basis of Eq. (A.4) and taking the inverse finite integral transform to Eq. (22), the Laplace-domain solution is obtained as

$$\hat{h}(\bar{r}, \bar{z}, p) = 2\sum_{n=1}^{\infty} \tilde{h}(\bar{r}, \beta_n, p)\cos(\beta_n \bar{z}) \tag{B.1}$$

with

$$\tilde{h}(\bar{r}, \beta_n, p) = \tilde{h}_1(p) \cdot \tilde{h}_2(p) \tag{B.2}$$

$$\tilde{h}_1(p) = \frac{\gamma}{(p^2 + \gamma^2)} \tag{B.3}$$

$$\tilde{h}_2(p) = -\varphi_1 \varphi_2 \tag{B.4}$$

$$\varphi_1 = K_0(\bar{r}\lambda)(\sin(\bar{z}_u \beta_n) - \sin(\bar{z}_l \beta_n))/(\beta_n \lambda K_1(\lambda)) \tag{B.5}$$

Hydrol. Earth Syst. Sci. Discuss., https://doi.org/10.5194/hess-2018-482
Manuscript under review for journal Hydrol. Earth Syst. Sci.
Discussion started: 1 November 2018

Hydrology and Earth System Sciences
Discussions

$$\varphi_2 = (\beta_n^2 + c^2)/(\beta_n^2 + c^2 + c) \tag{B.6}$$

where λ is defined in Eq. (23). Using the Mathematica function InverseLaplaceTransform, the inverse Laplace transform for $\tilde{h}_1(p)$ in Eq. (B.3) is obtained as

$$\bar{h}_1(\bar{t}) = \sin(\gamma\bar{t}) \tag{B.7}$$

The inverse Laplace transform for $\tilde{h}_2(p)$ in Eq. (B.4) is written as

$$\tilde{h}_2(\bar{t}) = \frac{1}{2\pi i}\int_{\rho-i\infty}^{\rho+i\infty} \tilde{h}_2(p)\ e^{p\bar{t}}dp \tag{B.8}$$

where ρ is a real number being large enough so that all singularities are on the LHS of the straight line from $(\rho, -i\infty)$ to $(\rho, i\infty)$ in the complex plane. The integrand $\tilde{h}_2(p)$ is a multiple-value function with a branch point at $p = -\mu\beta_n^2$ and a branch cut from the point along the negative real axis. In order to reduce $\tilde{h}_2(p)$ to a single-value function, we consider a modified Bromwich contour that contains a straight line $\overline{\mathrm{AB}}$, $\overline{\mathrm{CD}}$ right above the branch cut and $\overline{\mathrm{EF}}$ right below the branch cut, a semicircle with radius R, and a circle $\overset{\frown}{\mathrm{DE}}$ with radius r' in Fig. A1. According to the residual theory, Eq. (B.8) may be expressed as

$$\tilde{h}_2(\bar{t}) + \lim_{\substack{r'\to 0\\ R\to\infty}} \frac{1}{2\pi i}\Big[\int_B^C \tilde{h}_2(p)\ e^{p\bar{t}}dp + \int_C^D \tilde{h}_2(p)\ e^{p\bar{t}}dp + \int_D^E \tilde{h}_2(p)\ e^{p\bar{t}}dp +$$

$$\int_E^F \tilde{h}_2(p)\ e^{p\bar{t}}dp + \int_F^A \tilde{h}_2(p)\ e^{p\bar{t}}dp\Big] = 0 \tag{B.10}$$

where zero on the RHS is due to no pole in the complex plane. The integrations for paths $\overset{\frown}{\mathrm{BA}}$ (i.e. $\int_B^C \tilde{h}_2(p)\ e^{p\bar{t}}dp + \int_F^A \tilde{h}_2(p)\ e^{p\bar{t}}dp$) with $R \to \infty$ and $\overset{\frown}{\mathrm{DE}}$ (i.e. $\int_D^E \tilde{h}_2(p)\ e^{p\bar{t}}dp$) with $r' \to 0$ equal zero. The path $\overline{\mathrm{CD}}$ starts from $p = -\infty$ to $p = -\mu\beta_n^2$ and $\overline{\mathrm{EF}}$ starts from $p = -\mu\beta_n^2$ to $p = -\infty$. Eq. (B.10) therefore reduces to

$$\tilde{h}_2(\bar{t}) = -\frac{1}{2\pi i}\left(\int_{-\infty}^{-\mu\beta_n^2} \tilde{h}_2(p^+)e^{p^+\bar{t}}dp + \int_{-\mu\beta_n^2}^{-\infty} \tilde{h}_2(p^-)e^{p^-\bar{t}}dp\right) \tag{B.11}$$

where p^+ and p^- are complex numbers right above and below the real axis, respectively. Consider $p^+ = \zeta e^{i\pi} - \mu\beta_n^2$ and $p^- = \zeta e^{-i\pi} - \mu\beta_n^2$ in the polar coordinate system with the origin at $(-\mu\beta_n^2, 0)$ in the complex plane. Eq. (B.11) then becomes

Hydrology and Earth System Sciences
Open Access
Discussions

$$\tilde{h}_2(\bar{t}) = \frac{-1}{2\pi i}\int_0^\infty \tilde{h}_2(p^+)e^{p^+\bar{t}}dp - \tilde{h}_2(p^-)e^{p^-\bar{t}}d\zeta \quad \text{(B12)}$$

where p^+ and p^- lead to the same result of $p_0 = -\zeta - \mu\beta_n^2$ for a given ζ; $\lambda = \sqrt{p + \mu\beta_n^2}$ equals $\lambda_0 = \sqrt{\zeta}i$ for $p = p^+$ and $-\lambda_0$ for $p = p^-$. Note that $\tilde{h}_2(p^+)\ e^{p^+\bar{t}}$ and $\tilde{h}_2(p^-)\ e^{p^-\bar{t}}$ are in terms of complex numbers. The numerical result of the integrand in Eq. (B.12) must be a pure imaginary number that is exactly twice of the imaginary part of a complex number from $\tilde{h}_2(p^+)\ e^{p^+t}$ with $p^+ = p_0$ and $\lambda = \lambda_0$. The inverse Laplace transform for $\tilde{h}_2(p)$ can be written as

$$\tilde{h}_2(\bar{t}) = \frac{-1}{\pi}\int_0^\infty \mathrm{Im}\left(\varphi_1\varepsilon_2\ e^{p_0\bar{t}}\right)d\zeta \quad \text{(B.13)}$$

where $p = p_0$; $\lambda = \lambda_0$; φ_1 and ε_2 are respectively defined in Eqs. (B.5) and (24i). According to the convolution theory, the inverse Laplace transform for $\tilde{h}(\bar{r},\beta_n,p)$ is

$$\tilde{h}(\bar{r},\beta_n,\bar{t}) = \int_0^t \tilde{h}_2(\tau)\,\bar{h}_1(\bar{t}-\tau)d\tau \quad \text{(B.14)}$$

where $\bar{h}_1(\bar{t}-\tau) = \sin(\gamma(\bar{t}-\tau))$ based on Eq. (B.7); $\tilde{h}_2(\tau)$ is defined in Eq. (B.13) with $\bar{t} = \tau$. Eq. (B.14) can reduce to

$$\tilde{h}(\bar{r},\beta_n,\bar{t}) = \frac{-1}{\pi}\int_0^\infty \mathrm{Im}\left(\frac{\varphi_1\varepsilon_2(\gamma e^{p_0\bar{t}} - \gamma\cos(\gamma\bar{t}) - p_0\sin(\gamma\bar{t}))}{p_0^2+\gamma^2}\right)d\zeta \quad \text{(B.15)}$$

Substituting $\tilde{h}(\bar{r},\beta_n,p) = \tilde{h}(\bar{r},\beta_n,\bar{t})$ and $\hat{h}(\bar{r},\bar{z},p) = \bar{h}(\bar{r},\bar{z},\bar{t})$ into Eq. (B.1) and rearranging the result leads to

$$\bar{h}(\bar{r},\bar{z},\bar{t}) = \frac{-2}{\pi}\sum_{n=1}^{\infty}\int_0^\infty \cos(\beta_n\bar{z})\,\mathrm{Im}\left(\varepsilon_1\varepsilon_2\gamma e^{p_0\bar{t}}\right)d\zeta +$$

$$\frac{2}{\pi}\sum_{n=1}^{\infty}\int_0^\infty \cos(\beta_n\bar{z})\,\mathrm{Im}\left(\varepsilon_1\varepsilon_2(\gamma\cos(\gamma\bar{t}) + p_0\sin(\gamma\bar{t}))\right)d\zeta \quad \text{(B.16)}$$

where ε_1 and ε_2 are defined in Eqs. (24h) and (24i); the first RHS term equals $\bar{h}_{\exp}(\bar{r},\bar{z},\bar{t})$ defined in Eq. (24b); the second term is denoted as $\bar{h}_{\mathrm{SHM}}(\bar{r},\bar{z},\bar{t})$ defined in Eq. (24c). Finally, the complete solution is expressed as Eqs. (24a) – (24k).

Appendix C: Weber transform

Applying the Weber transform to $\bar{H}$ of the model, Eqs. (27) – (31), yields

Hydrol. Earth Syst. Sci. Discuss., https://doi.org/10.5194/hess-2018-482
Manuscript under review for journal Hydrol. Earth Syst. Sci.
Discussion started: 1 November 2018

Hydrology and Earth System Sciences
Open Access
Discussions

$$\widetilde{H}(\xi) = \mathcal{W}\{\bar{H}\} = \int_1^\infty \bar{H}\ \bar{r}\ \Omega\ dr \tag{C1}$$

where Ω is defined in Eq. (39b). With the integration by parts, the transform has the property that

$$\mathcal{W}\left\{\frac{\partial^2 \bar{H}}{\partial \bar{r}^2} + \frac{1}{\bar{r}}\frac{\partial \bar{H}}{\partial \bar{r}}\right\} = -\xi^2 \widetilde{H} - \frac{2}{\pi\xi}\frac{d\bar{H}}{d\bar{r}}\bigg|_{\bar{r}=1} \tag{C2}$$

where the second RHS term represents the Neumann boundary condition Eq. (28). The formula for the inversion can be written as

$$\bar{H} = \mathcal{W}^{-1}\{\widetilde{H}\} = \int_0^\infty \widetilde{H}\ \xi\ \Omega\ d\xi \tag{C3}$$

Table 1. The present solution and its special cases

Well screen	Transient flow		Pseudo-steady state flow	
	Unconfined aquifer	Confined aquifer	Unconfined aquifer	Confined aquifer
Partial	Solutions 1 and 2	Solution 3	Solutions 4 and 5	Solution 6
Full	Solutions 1 and 2[a]	Solution 3[a,b]	Solutions 4 and 5[a]	Solution 6[a,b]

Solution 1 consists of Eqs. (24a) – (24k) with the roots of Eq. (19) and $c_0 = a_1 p_0/(p_0 + a_2)$ for DGD.

Solution 2 is the same as solution 1 but has $c_0 = a p_0$ for IGD.

Solution 3 equals solution 1 with Eqs. (25a) – (25d) and $\beta_n = 0,\ \pi,\ 2\pi, \ldots,\ n\pi$.

Solution 4 is the component $\bar{h}_{\mathrm{SHM}}$ of solution 1 for DGD.

Solution 5 consists of Eqs. (40a) – (40e) for IGD.

Solution 6 consists of Eqs. (40a) – (40e) with $\bar{H}(\bar{r}, \bar{z})$ defined by Eq. (45).

[a] $\bar{z}_u = 1$ and $\bar{z}_l = 0$ for fully screened well

[b] The solution is independent of elevation due to fully screened well.

Hydrology and Earth System Sciences
Open Access
Discussions

626 **Table 2.** Hydraulic parameters estimated by the present solution for OPT data from the Savannah River site

Observation well	Present solution	T (m²/s)	S	K_z (m/s)	S_y	ε (s⁻¹)	SEE	ME
				Surficial Aquifer				
101D	Solution 3[a]	9.27×10^{-4}	2.44×10^{-3}	-	-	-	0.018	-5.56×10^{-3}
	Solution 6[b]	9.18×10^{-4}	2.33×10^{-3}	-	-	-	0.018	-2.20×10^{-4}
	Solution 4[c]	4.61×10^{-4}	3.95×10^{-3}	7.38×10^{-6}	2.23×10^{-3}	1.06×10^{-2}	0.018	-2.20×10^{-4}
	Solution 5[c]	5.25×10^{-4}	1.09×10^{-3}	2.61×10^{-5}	5.49×10^{-3}	-	0.019	-2.30×10^{-4}
102D	Solution 3[a]	9.13×10^{-4}	1.76×10^{-3}	-	-	-	0.010	-4.38×10^{-3}
	Solution 6[b]	9.17×10^{-4}	1.67×10^{-3}	-	-	-	0.011	9.57×10^{-4}
	Solution 4[c]	9.57×10^{-5}	7.85×10^{-4}	3.68×10^{-6}	4.95×10^{-3}	2.38×10^{-3}	0.011	9.57×10^{-4}
	Solution 5[c]	9.49×10^{-5}	3.25×10^{-4}	4.67×10^{-6}	4.68×10^{-3}	-	0.011	9.50×10^{-4}
				Barnwell-McBean Aquifer				
201C	Solution 3[a]	5.86×10^{-5}	7.07×10^{-4}	-	-	-	0.232	0.046
	Solution 6[b]	6.03×10^{-5}	6.54×10^{-4}	-	-	-	0.363	0.281

627 [a] transient confined flow
628 [b] PSS confined flow
629 [c] PSS unconfined flow

Hydrology and Earth System Sciences
Open Access
Discussions

Figures

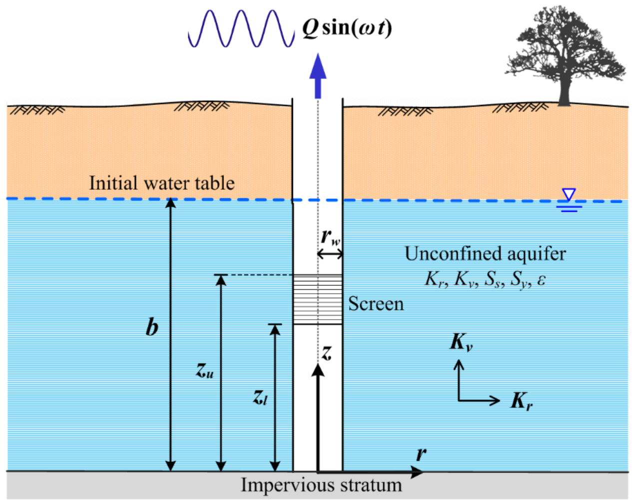

Figure 1. Schematic diagram for oscillatory pumping test at a partially screened well of finite radius in an unconfined aquifer.

Hydrol. Earth Syst. Sci. Discuss., https://doi.org/10.5194/hess-2018-482
Manuscript under review for journal Hydrol. Earth Syst. Sci.
Discussion started: 1 November 2018

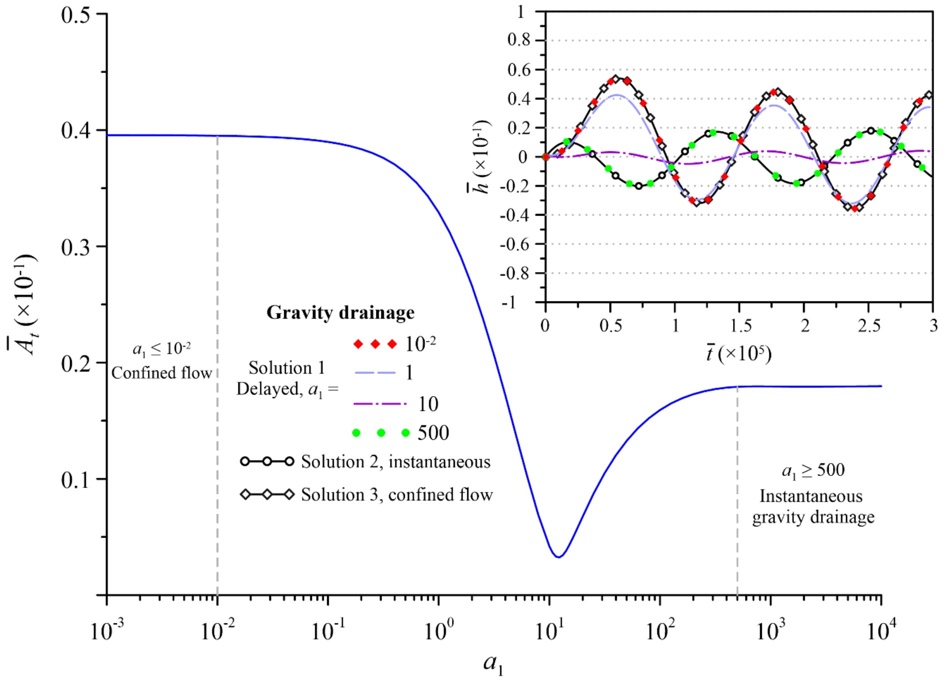

Figure 2. Influence of delayed gravity drainage on the dimensionless amplitude $\bar{A}_t$ and transient head $\bar{h}$ at $\bar{r} = 1$, $\bar{z} = 1$ predicted by solution 1 for different magnitudes of a_1 related to the influence.

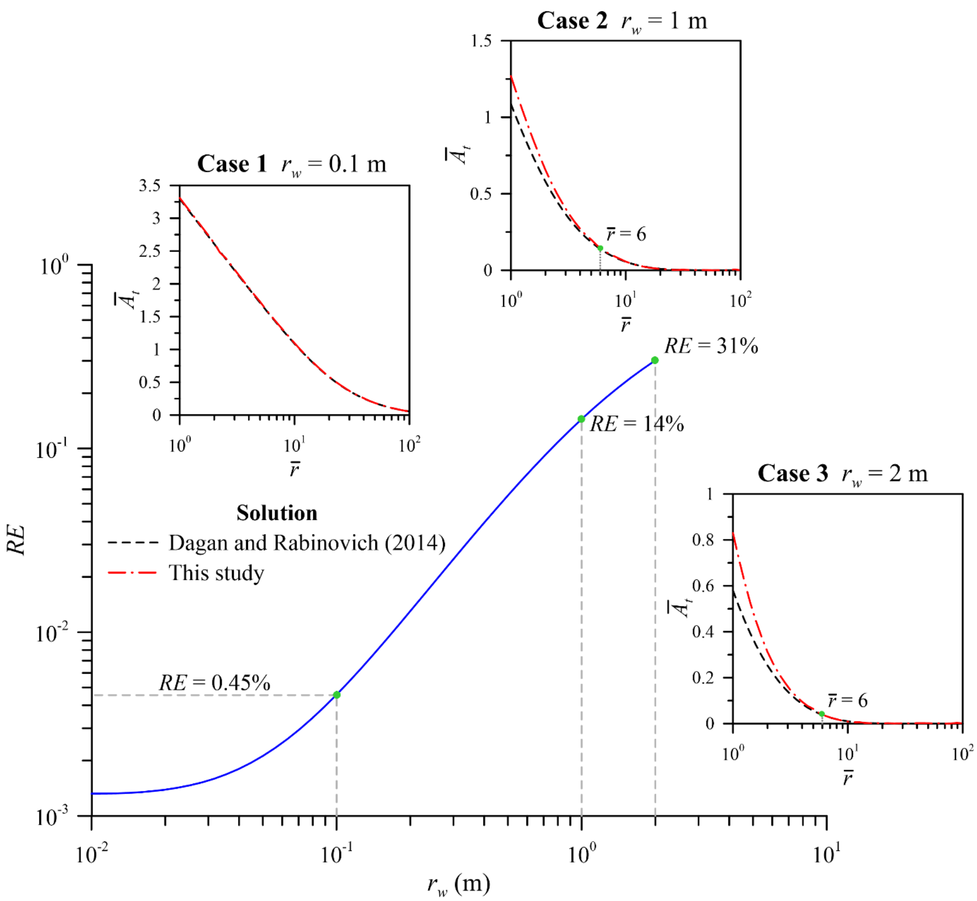

Figure 3. Relative error (RE) on the dimensionless amplitudes $\bar{A}_t$ at the rim of the pumping well (i.e., $r = r_w$) predicted by the Dagan and Rabinovich (2014) solution and the IGD solution 2. The well radius is assumed infinitesimal in the Dagan and Rabinovich (2014) solution and finite in our solution.

Hydrol. Earth Syst. Sci. Discuss., https://doi.org/10.5194/hess-2018-482
Manuscript under review for journal Hydrol. Earth Syst. Sci.
Discussion started: 1 November 2018

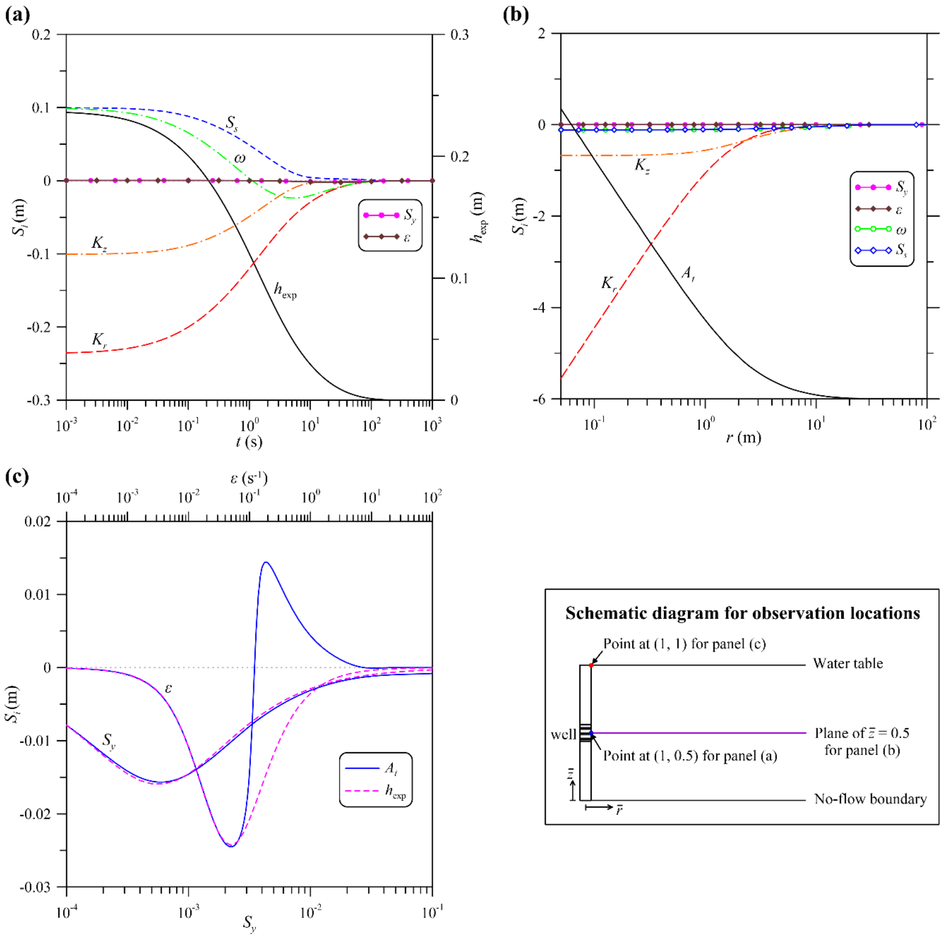

Figure 4. The normalized sensitivity coefficient S_i associated with (a) the exponential component h_{exp} of solution 1 and (b) the SHM amplitude A_t for parameters K_r, K_z, S_s, S_y, ω and ε. The observation locations for panels (a) and (b) are under water table (i.e., $\bar{z} = 0.5$). Panel (c) displays the curves of S_i of h_{exp} and A_t at water table (i.e., $\bar{z} = 1$) versus S_y and ε.

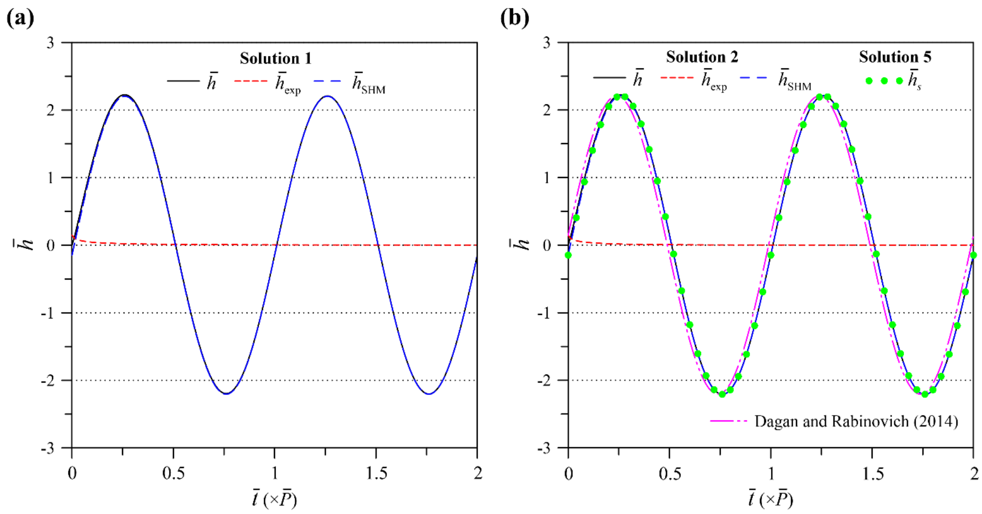

Figure 5. Heads fluctuations at $\bar{r} = 6$ predicted by (a) DGD solution 1 and (b) IGD solution 2. Solutions 1 and 2 are expressed as $\bar{h} = \bar{h}_{\mathrm{exp}} + \bar{h}_{\mathrm{SHM}}$ for transient flow. IGD solution 5 expressed as $\bar{h}_s = \bar{A}_s \cos(\gamma t - \phi_s)$ accounts for PSS flow.

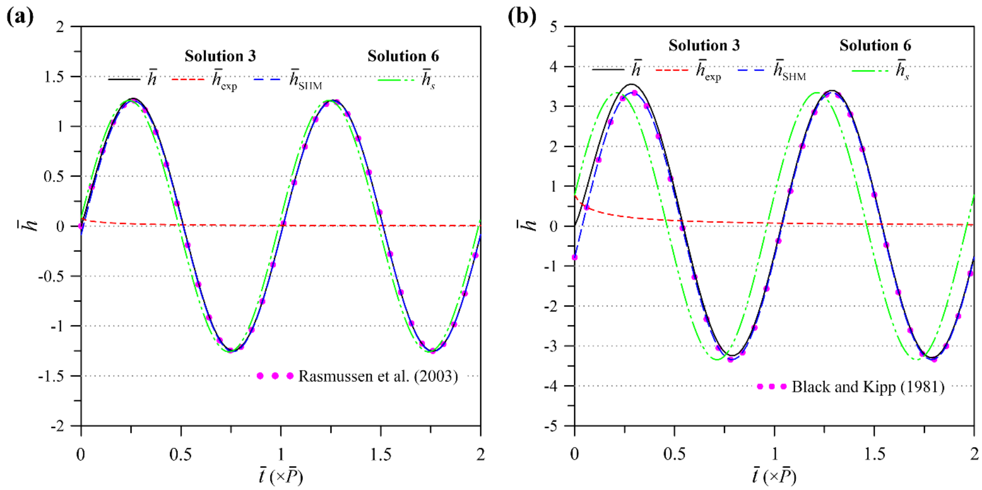

Figure 6. Heads fluctuations at $\bar{r} = 6$ predicted by solutions 3 and 6 for (a) partially-screend pumping well and (b) fully-screened pumping well. Solution 3 is expressed as $\bar{h} = \bar{h}_{\exp} + \bar{h}_{\mathrm{SHM}}$ for transient flow. Solution 6 expressed as $\bar{h}_s = \bar{A}_s \cos(\gamma t - \phi_s)$ accounts for PSS flow.

Hydrol. Earth Syst. Sci. Discuss., https://doi.org/10.5194/hess-2018-482
Manuscript under review for journal Hydrol. Earth Syst. Sci.
Discussion started: 1 November 2018

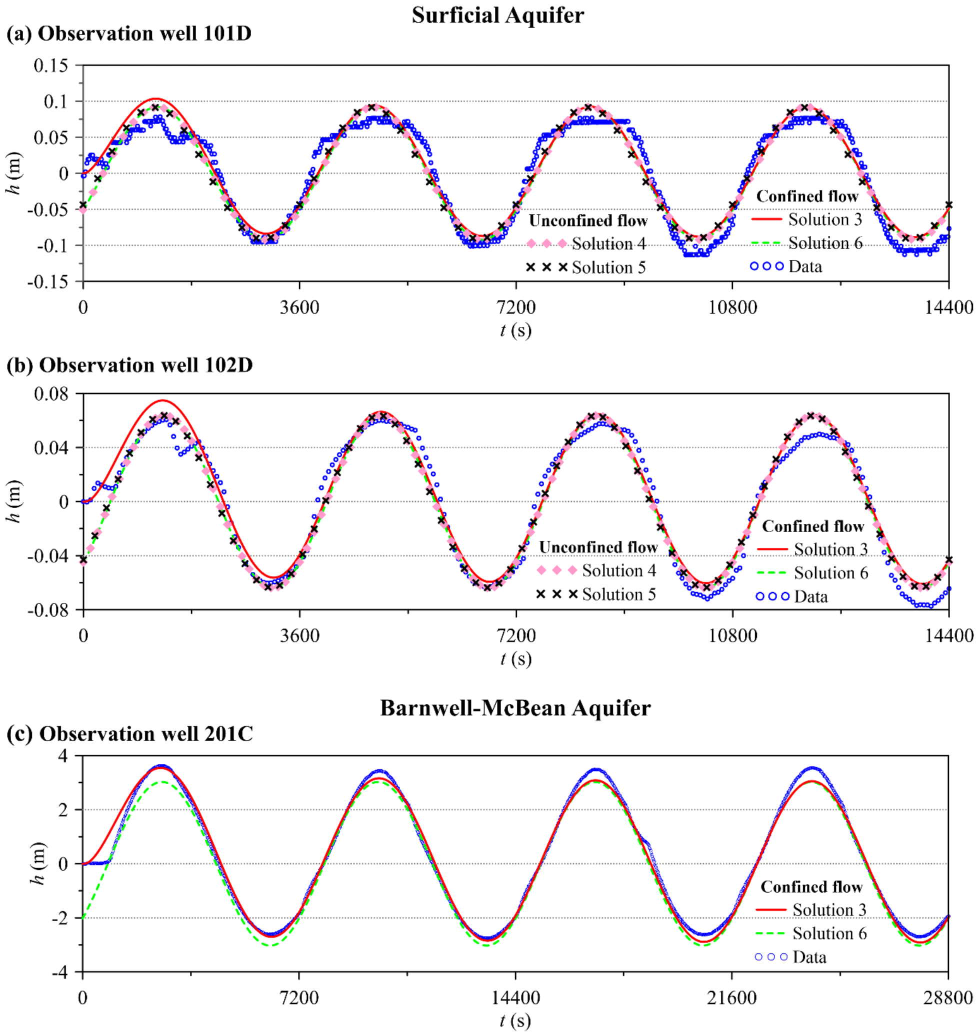

Figure 7. Comparision of field observation data with head fluctuations predicted by the present solution. Solutions 3 and 6 represent transient and PSS confined flows, respectively. PSS solutions 4 and 5 stand for DGD and IGD conditions, respectively.

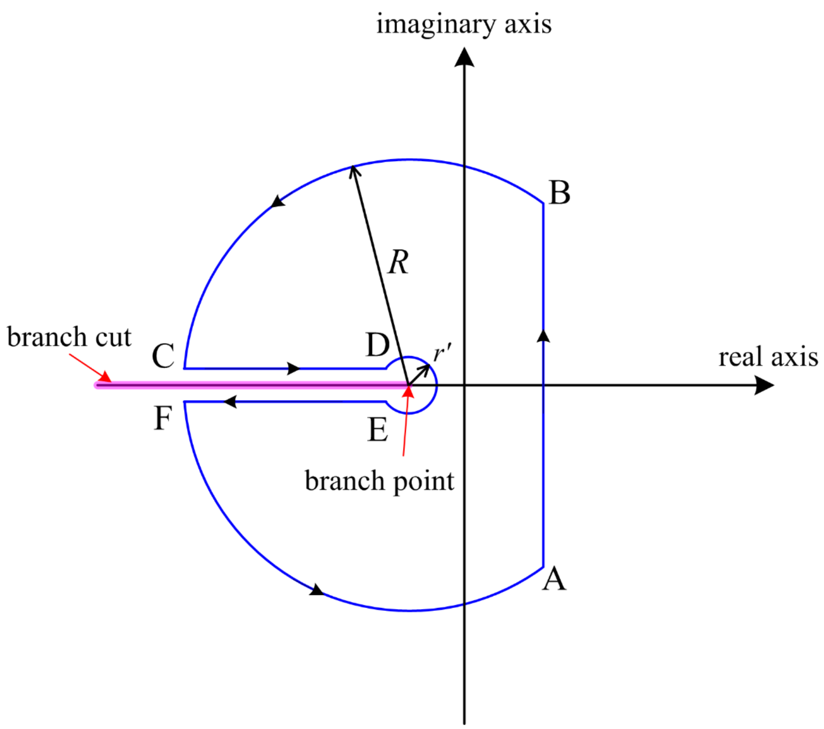

Figure A1. Modified Bromwich contour for the inverse Laplace transform to a multiple-value function with a branch point and a branch cut